J. Fluid Mech. (1984), *vol.* 145, *pp.* 287–304
Printed in Great Britain

Line momentum source in shallow inviscid fluid

By JOSEPH H. W. LEE
Department of Civil Engineering, University of Hong Kong, Hong Kong

AND MICHAEL D. GREENBERG
Department of Mechanical and Aerospace Engineering, University of Delaware, Newark, Delaware 19716

(Received 28 June 1983)

An array of closely spaced, aligned, turbulent, incompressible jets is effectively simulated by a line momentum source. In a shallow inviscid fluid, such a source induces a predominantly two-dimensional non-diffusive flow which is irrotational except along lines of velocity discontinuity downstream of the source. The flow can be generated by a distribution of line vortices of unknown strength along the unknown slipstreamlines. Based upon this vortex model, kinematic and dynamic conditions along the slipstreamlines are formulated, and the two resulting nonlinear singular integral equations are solved numerically using a Newton–Raphson-type iterative collocation method.

The flow field shows a marked resemblance to that induced by a nonlinear actuator disk. For the case of no ambient current, experimental results indicate that the slipstreamlines emanate from points which are close to, but not at the ends of, the source. As the ambient current strength increases, a dividing streamline appears in the induced sink flow upstream of the source, and the points from which the slipstreamlines emanate move closer to the ends of the source. Further increases in the current strength result in the smooth blending of this dividing streamline with the slipstreamline.

Laboratory experiments performed in a shallow water basin confirm all of the features predicted by the theory.

1. Introduction

The injection of an aligned series of submerged, high-velocity, turbulent, incompressible jets into a shallow inviscid fluid of similar constant density ρ is shown schematically in figure 1. The ambient fluid, infinite in horizontal extent and of uniform (undisturbed) depth H, is bounded by a flat solid bottom and a free surface. When closely spaced, these multiple jets form a line momentum source which effects rapid mixing with the ambient fluid and significantly modifies the ambient flow.

Such multiple-jet configurations are increasingly being adopted as mixing devices for the disposal of cooling water from steam electric-power stations located near shallow coastal waters. With source flows typically of the order of 100 m^3/s and discharge jet velocities as high as 5 m/s or more, the large momentum imparted in depths of 5–10 m can lead to flows comparable to those in large rivers entering the coastal zone. The velocities so induced may also have significant effects upon coastal sediment transport and coastal morphology over large regions.

Whereas turbulent incompressible free jets and their various applications have been studied extensively (e.g. Abramovich 1963; Schlichting 1968; Albertson *et al.* 1950;

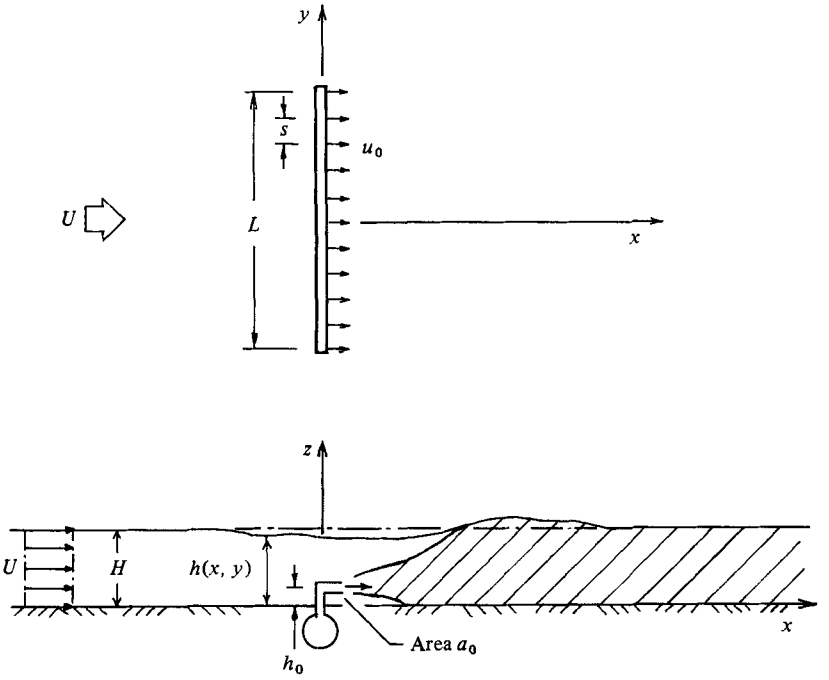

FIGURE 1. Line momentum source consisting of a series of high-velocity, turbulent, incompressible jets in shallow fluid.

Fischer *et al.* 1979), the mechanics of the flow generated by the interaction of multiple jets in the presence of a free surface has received scant attention. Consider the case in which the ambient fluid is otherwise quiescent. In the absence of boundary effects, it has been shown experimentally by Knystautas (1964) that the closely spaced, multiple, interfering, turbulent, axisymmetric jets acting independently lose their individual character and form an essentially two-dimensional jet by approximately twelve jet spacings downstream. In a fluid confined vertically, however, the outer jets deflect toward the centreline of the jet group as a result of the pressure field set up by the potential entrainment flow outside the individual jets (Taylor 1958). Such tendency for the jets to merge has been observed experimentally by Baines & Keffer (1974) in a study of an axisymmetric group of air jets, by Miller & Comings (1960) for dual slot jets, and also by Lee & Jirka (1979) in experimental investigations of shallow-water jets. This zone of jet interference, in which the source momentum is transferred to the ambient fluid by jet diffusion, is also associated with an adverse pressure gradient for increasing x. The length x_m of this merging-jet region depends upon the depth H, the jet spacing s and the height h_0 of the jets above the bottom. For closely spaced jets near the bottom, the length can be estimated as $x_m \approx H/k$, where k is the spreading angle for a free turbulent jet, neglecting the effects of pressure gradient and jet interference. For $k \approx 0.1$ (Schlichting 1968; Davis & Winarto 1980) $x_m \approx 10H$.

If the source length L is large compared with the depth H, $L/H \gg 1$, the highly complicated three-dimensional flow in the momentum-transfer region will not be important in an account of the flow leading to the ultimate two-dimensional jet, and a horizontal flow situation can be assumed in which the overall induced flow is determined by the multiple jets acting together as a line momentum source. This paper is concerned with the two-dimensional velocity field generated by such a line

momentum source aligned with an ambient current U in a shallow fluid. A pressure discontinuity is created, across the line source, by the momentum flux per unit length ρm, and the resulting flow is essentially a two-dimensional analogue of the nonlinear actuator disk encountered in propeller theory. A qualitative indication of the flow within the slipstream was given earlier by Lee (1980), based upon an *a priori* assumption of the induced velocity distribution at the source line.

2. Theoretical development

2.1. *Development of vortex model*

Assuming that $L/H \gg 1$, we adopt the results of the classical shallow-water theory, namely that the flow is planar and that the pressure $p(x, y, z)$ is given by the hydrostatic distribution

$$p = \rho g[h(x, y) - z], \tag{1}$$

where ρ is the fluid mass density, g is the acceleration due to gravity, and $h(x, y)$ is the free-surface height above the bottom. (However, we also require that L/H not be excessively large, say $L/H < 100$, so that bottom-frictional dissipation can be neglected.)

Applying the Bernoulli equation along the bottom ($z = 0$), first between a point far upstream and a point $(0-, y, 0)$ on the upstream side of the line source, then between $(0+, y, 0)$ and a point far downstream, subtraction and addition of these two equations yields

$$\Delta h(y) = \frac{1}{2g}[u_\infty^2 - U^2 + u^2(0-, y) - u^2(0+, y)] \tag{2}$$

and

$$\tfrac{1}{2}[h(0+, y) + h(0-, y)] = H + \frac{1}{4g}[U^2 + u_\infty^2 - u^2(0-, y) - u^2(0+, y) - 2v^2(0, y)], \tag{3}$$

where the fluid velocity $\boldsymbol{q} = u(x, y)\,\hat{\boldsymbol{\imath}} + v(x, y)\hat{\boldsymbol{\jmath}} \sim u_\infty(y)\,\hat{\boldsymbol{\imath}}$ as $x \to \infty$ within the slipstream, and

$$\Delta h(y) \equiv h(0+, y) - h(0-, y) \quad (|y| < \tfrac{1}{2}L). \tag{4}$$

(Note that we have not written $u_\infty^2(y)$ in (2) and (3), since u_∞^2 is evaluated on the streamline passing through $(0, y)$, and the y-coordinate of this streamline decreases as $x \to \infty$, as sketched in figure 2.) In deriving (2) and (3) we have noted that $v(0+, y) = v(0-, y)$, but have allowed for $u(0+, y) \neq u(0-, y)$ by virtue of the fact that the multiple jets act as a line mass source (as well as a line momentum source).

At this point we introduce two assumptions. Observing that the mass and momentum inputs are independent quantities, and that the momentum-induced flow is typically much larger than the source-induced flow, we assume that the multiple jets act as a line momentum source but *not* as a line mass source. Subject to this assumption, which will be made precise at the end of §2.2, (2) becomes

$$\Delta h(y) = \frac{1}{2g}(u_\infty^2 - U^2). \tag{5}$$

Secondly we assume that

$$q^2/gH \ll 1 \tag{6}$$

everywhere in the field, as occurs under typical operating conditions, in which case (3) becomes

$$\tfrac{1}{2}[h(0+,y)+h(0-,y)] = H. \tag{7}$$

Next we apply a momentum balance just across the line source (i.e. on the fluid between $x = 0-$ and $x = 0+$, between y and $y+\Delta y$, and between $z = 0$ and $z = h(x,y)$) and, using (6) and (7), obtain

$$\Delta h(y) = \frac{m}{gH}, \tag{8}$$

where $m = u_0^2 a_0/s$ is a constant. Here u_0 is the jet velocity and a_0 is the jet cross-sectional area (figure 1). In physical terms, (8) expresses a force balance between the net pressure force $\rho g H \Delta h(y)$ per unit y-length and the force ρm per unit y-length exerted on the fluid by the jet nozzles.

From (5) and (8) follows the important conclusion that

$$u_\infty(y) = \text{constant} \equiv u_\infty \tag{9}$$

within the slipstream.

Now $\boldsymbol{q} \sim u_\infty \hat{\boldsymbol{\imath}}$ implies that $\boldsymbol{\nabla} \times \boldsymbol{q} \to \boldsymbol{0}$ as $x \to \infty$ within the slipstream. From Helmholtz's theorem it follows that $\boldsymbol{\nabla} \times \boldsymbol{q} = \boldsymbol{0}$ everywhere within the slipstream. Likewise, $\boldsymbol{\nabla} \times \boldsymbol{q} = \boldsymbol{0}$ everywhere outside the slipstream since $\boldsymbol{q} \sim U\hat{\boldsymbol{\imath}}$ at infinity, so that the vorticity springing from the momentum source must be confined to the slipstream boundary $y = \pm f(x)$ $(0 < x < \infty)$, as sketched in figure 2. The unknowns of the problem may thus be considered as the slipstream boundary shape $f(x)$ and the vortex density $\gamma(x)$ (i.e. the circulation per unit x-length) along that boundary.

Before proceeding, let us re-emphasize the independence of the momentum and mass inputs by noting that we can increase u_0 and decrease a_0 such that Δh (which, according to (8), is proportional to the momentum flux) is held fixed while $u_0 a_0$ (and hence the mass flux) tends to zero. Finally we note that our shallow-water-theory assumptions must break down in the neighbourhood of the source line owing to the jump discontinuity in $h(x,y)$, though this local breakdown may be no more serious than our willingness to 'smear out' the discrete inputs into a continuous source line.

2.2. *Governing equations*

There are two conditions governing $f(x)$ and $\gamma(x)$: a kinematic condition that the slipstream boundaries $y = \pm f(x)$ $(0 < x < \infty)$ be streamlines, and a dynamic condition that the pressure be continuous across these 'slipstreamlines'. Now the stream function $\psi(x,y)$ induced at (x,y) by a vortex of unit strength (positive counter-clockwise) at (ξ,η) is

$$\psi(x,y) = -\frac{1}{4\pi} \ln[(\xi-x)^2+(\eta-y)^2]. \tag{10}$$

Thus, superimposing the free stream U and the slipstreamline vorticity, we have

$$\psi(x,y) = Uy + \int_0^\infty G[\xi, f(\xi); x, y]\, \gamma(\xi)\, \mathrm{d}\xi, \tag{11}$$

where the kernel is

$$G(\xi,\eta;x,y) = \frac{1}{4\pi} \ln \frac{(\xi-x)^2+(\eta+y)^2}{(\xi-x)^2+(\eta-y)^2}. \tag{12}$$

As $x \to \infty$ the velocity induced by the vortex sheets is the same as that induced by two *straight* doubly infinite vortex sheets: one along $y = f_\infty$ with vortex density γ_∞

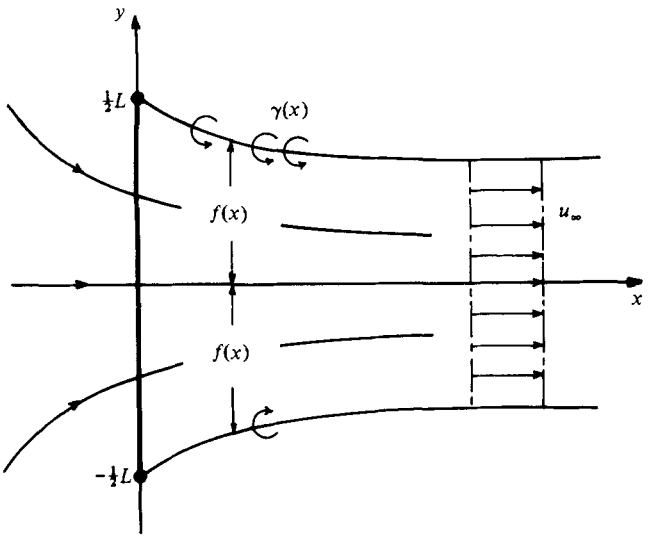

FIGURE 2. Vortex model of slipstream.

counterclockwise, and one along $y = -f_\infty$ with vortex density γ_∞ clockwise, where f_∞ and γ_∞ denote the asymptotic values of $f(x)$ and $\gamma(x)$ as $x \to \infty$. The velocity field (u, v) induced by such sheets is easily shown to be $(0, 0)$ for $|y| > f_\infty$ and $(\gamma_\infty, 0)$ for $|y| < f_\infty$. Thus

$$\psi[x, f(x)] \sim (U + \gamma_\infty) f_\infty = u_\infty f_\infty \tag{13}$$

as $x \to \infty$, and so the kinematic condition $\psi[x, f(x)] =$ constant becomes

$$u_\infty f_\infty = U f(x) + \int_0^\infty G[\xi, f(\xi); x, f(x)]\, \gamma(\xi)\, \mathrm{d}\xi. \tag{14}$$

Turning to the dynamic condition, if we write Bernoulli's equation (along $z = 0$) twice – once on either side of the slipstreamline – and difference these equations, we obtain

$$\begin{aligned} \frac{m}{H} &= \tfrac{1}{2}\{q^2[x, f(x)-] - q^2[x, f(x)+]\} \\ &= \tfrac{1}{2}\{q[x, f(x)-] + q[x, f(x)+]\}\{q[x, f(x)-] - q[x, f(x)+]\} \\ &= q[x, f(x)]\, \gamma_s(x), \end{aligned} \tag{15}$$

where $\gamma_s(x)$ is the circulation per unit arclength s (measured positive downstream), and is related to $\gamma(x)$, the circulation per unit x-length, according to

$$\gamma(x) = \gamma_s(x) \frac{\mathrm{d}s}{\mathrm{d}x}. \tag{16}$$

Thus (15) becomes

$$\frac{m}{H} = q[x, f(x)] \frac{\mathrm{d}x}{\mathrm{d}s} \gamma(x),$$

or

$$\frac{m}{H} = u[x, f(x)]\, \gamma(x). \tag{17}$$

As $x \to \infty$ (17) becomes

$$\frac{m}{H} = (U + \tfrac{1}{2}\gamma_\infty)\gamma_\infty, \tag{18}$$

so that we may solve, *a priori*, for γ_∞ in terms of known quantities, as

$$\gamma_\infty = \left(U^2 + \frac{2m}{H}\right)^{\frac{1}{2}} - U. \tag{19}$$

Finally, $u = \partial\psi/\partial y$, so we have, as the final form of the dynamic boundary condition,

$$(U + \tfrac{1}{2}\gamma_\infty)\frac{\gamma_\infty}{\gamma(x)} = U + \int_0^\infty G_y[\xi, f(\xi); x, f(x)]\,\gamma(\xi)\,\mathrm{d}\xi. \tag{20}$$

Equations (14) and (20) are coupled, nonlinear, singular integral equations in the unknowns $f(x)$ and $\gamma(x)$; the kernels admit the singular behaviour

$$G[\xi, f(\xi); x, f(x)] = O[\ln(\xi - x)], \quad G_y[\xi, f(\xi); x, f(x)] = O\left(\frac{1}{\xi - x}\right) \tag{21a,b}$$

as $\xi \to x$.

We now non-dimensionalize as follows: $x^* = x/\frac{1}{2}L$ and similarly for ξ, y, f and f_∞; $\gamma^* = \gamma/\gamma_\infty$; $U^* = U/u_\infty$, where we recall that $u_\infty = U + \gamma_\infty$. *Henceforth omitting the asterisks*, for notational simplicity, (14) and (20) become

$$\frac{f_\infty - Uf(x)}{1 - U} = \int_0^\infty G[\xi, f(\xi); x, f(x)]\,\gamma(\xi)\,\mathrm{d}\xi \tag{22}$$

and

$$\frac{1}{1 - U}\left(\frac{1 + U}{2\gamma(x)} - U\right) = \int_0^\infty G_y[\xi, f(\xi); x, f(x)]\,\gamma(\xi)\,\mathrm{d}\xi \tag{23}$$

respectively.

Finally, now that we have obtained the induced velocity

$$u_\infty - U = \gamma_\infty = [U^2 + (2m/H)]^{\frac{1}{2}} - U,$$

for reference, we can state our assumption that the mass source is negligible in terms of known quantities in the form $u_0 a_0/Hs \ll u_\infty - U$, or

$$\epsilon \equiv \frac{u_0 a_0}{Hs\left[\left(U^2 + \dfrac{2m}{H}\right)^{\frac{1}{2}} - U\right]} \ll 1. \tag{24}$$

2.3. *Numerical solution*

The governing equations (22) and (23) are solved numerically using a Newton–Raphson-type iterative collocation scheme previously employed in nonlinear actuator-disk theory (Greenberg 1972).

First we express the nth iterate of the slipstreamline shape in the form

$$f^{(n)}(x) = 1 + \sum_{j=1}^{M} b_j^{(n)}\,[f_j(x) - f_j(0)], \tag{25}$$

where the $f_j(x)$ basis functions are chosen as

$$f_j(x) = \mathrm{e}^{-jx}. \tag{26}$$

For the vorticity we express

$$\gamma^{(n)}(x) = T^{(n)}(x)\left[1+\sum_{j=1}^{N} a_j^{(n)} g_j(x)\right], \tag{27}$$

where

$$T^{(n)}(x) = \left[1+[f^{(n)\prime}(x)]^2\right]^{\frac{1}{2}}, \tag{28}$$

and the $g_j(x)$ basis functions are chosen as

$$g_j(x) = \begin{cases} x^{-\frac{1}{2}}\mathrm{e}^{-3x} & (j=1), \\ x^{-0.86+0.52j}\mathrm{e}^{-3x} & (j \geqslant 2). \end{cases} \tag{29}$$

The reason we include the $T^{(n)}(x)$ in (27) is that the square-bracketed portion of the right-hand side is then the circulation per unit *arc*length, which should be more gradually varying than $\gamma^{(n)}(x)$, near $x = 0$, in the event that there is a strong slipstream contraction at the 'lip', i.e. in the neighbourhood of $x = 0$. And the $x^{-\frac{1}{2}}$ is included in $g_1(x)$ because we need to allow for the square-root singularity dictated by the singular nature of the kernels, (21), as in the classical two-dimensional airfoil theory.

Rather than use (22) and (23), together, to solve for $f^{(n+1)}$ and $\gamma^{(n+1)}$, we use (22) to compute $f^{(n+1)}$, then (23) to compute $\gamma^{(n+1)}$, and so on. Though this scheme may compromise speed of convergence, it substantially reduces the computation time per iteration, and simplifies the programming. Following the quasilinearization idea of Newton–Raphson, we expand

$$G^{(n+1)} \approx G^{(n)} + \alpha G_\eta^{(n)}[f^{(n+1)}(\xi) - f^{(n)}(\xi)] + \beta G_y^{(n)}[f^{(n+1)}(x) - f^{(n)}(x)] \tag{30a}$$

in (22), and

$$\frac{1}{\gamma^{(n+1)}} \approx \frac{1}{\gamma^{(n)}} - \frac{1}{[\gamma^{(n)}]^2}(\gamma^{(n+1)} - \gamma^{(n)}) \tag{30b}$$

in (23), where α and β are included as 'convergence factors', and $G_\eta^{(n)}$, for example, denotes $G_\eta[\xi, f^{(n)}(\xi); x, f^{(n)}(x)]$. Thus (22) and (23) become

$$\begin{aligned} \frac{f_\infty^{(n+1)} - U f^{(n)}(x)}{1-U} = &\int_0^\infty G^{(n)}\gamma^{(n)}\,\mathrm{d}\xi \\ &+\alpha\int_0^\infty G_\eta^{(n)}(f^{(n+1)} - f^{(n)})\,\gamma^{(n)}\,\mathrm{d}\xi \\ &+\beta[f^{(n+1)}(x) - f^{(n)}(x)]\int_0^\infty G_y^{(n)}\,\gamma^{(n)}\,\mathrm{d}\xi \end{aligned} \tag{31}$$

and

$$\frac{1}{(1-U)}\left[\frac{1+U}{2}\left\{\frac{1}{\gamma^{(n)}(x)} - \frac{\gamma^{(n+1)}(x) - \gamma^{(n)}(x)}{[\gamma^{(n)}(x)]^2}\right\} - U\right] = \int_0^\infty G_y^{(n)}\,\gamma^{(n+1)}\,\mathrm{d}\xi \tag{32}$$

respectively. Putting (25)–(29) into (31) and requiring satisfaction at M prescribed points x_{kj} $(j = 1, \ldots, M)$ yields M linear algebraic equations in the new 'shape coefficients' $b_j^{(n+1)}$ $(j = 1, \ldots, M)$. Similarly, putting (25)–(29) into (32) and requiring satisfaction at N points x_{dj} $(j = 1, \ldots, N)$ yields N linear algebraic equations in the new 'circulation coefficients' $a_j^{(n+1)}$ $(j = 1, \ldots, N)$. Details of the algorithm are given in Lee (1982).

Initializing $f^{(0)}(x) = 1$ and $\gamma^{(0)}(x) = 1$, the scheme is found to work for all ambient currents $0 \leqslant U < 1$, with optimal convergence rate corresponding to the choice $\alpha \approx 0$, $\beta \approx 2$. This result may be interpreted physically, for if $\alpha = 0$ and $\beta = 2$ then

$$\int_0^\infty G^{(n+1)}\gamma^{(n)}\,\mathrm{d}\xi = \int_0^\infty G^{(n)}\gamma^{(n)}\,\mathrm{d}\xi + 2(f^{(n+1)} - f^{(n)})\int_0^\infty G_y^{(n)}\,\gamma^{(n)}\,\mathrm{d}\xi. \tag{33}$$

The first term on the right-hand side of (33) is the slipstream flow (over the half-slipstream $0 \leqslant y \leqslant f(x)$) passing the section $\xi = x$, induced by $\gamma^{(n)}$ on $f^{(n)}$. The second term provides a correction to this flow due to the iterative change in slipstream width; $\int_0^\infty G_y^{(n)}\,\gamma^{(n)}\,\mathrm{d}\xi$ is the x-velocity *on* the slipstreamline, which is approximately half the x-velocity just *inside* the slipstream (exactly, in fact, as $x \to \infty$), so that $2\int_0^\infty G_y^{(n)}\,\gamma^{(n)}\,\mathrm{d}\xi$ is approximately the x-velocity just inside the slipstream.

The choices $M = 8$, $N = 9$ were found to suffice, and convergence was achieved in at most seven iterations, when the successive iterates $f^{(n)}$, $f^{(n+1)}$ and $\gamma^{(n)}$, $\gamma^{(n+1)}$ were asked to differ by less than 0.5 % at a large number of x-points. The left- and right-hand sides of (22) and (23) were then found to agree, uniformly in x, to at least 3 significant digits.

2.4. *Numerical results*

Results are displayed in figure 3 and table 1 for the case $U = 0$, and the corresponding flow field is shown in figure 4(*a*); the cases $U = 0.1$ and $U = 0.286$ are depicted in figure 4(*b*, *c*) respectively. Finally, the u- and v-velocity distributions at the line source ($x = 0$, $0 < y < 1$) are shown in figure 5.

The following points may be made.

(i) The slipstream contraction is strongest for $U = 0$, and reduces to zero as $U \to 1$. As a quantitative check, we note that it may be shown, *a priori*, by a global x-momentum balance, that

$$f_\infty = \tfrac{1}{2}(1 + U), \tag{34}$$

so that $U = 0$ gives $f_\infty = 0.5$, i.e. a 50 % contraction. By comparison, our computed value of f_∞ (for $U = 0$) is 0.554, and the agreement becomes closer and closer as U increases (table 2). The difference between the iteratively computed f_∞ and that computed from (34) is further discussed in §3.2.

(ii) The ultimate slipstream values (i.e. those at $x = \infty$) are essentially attained – even for the most severe case $U = 0$ – by around $x = 2$.

(iii) We see from figure 4(*a*) that if $U = 0$ then *all* of the flow is drawn through the line source. If, for reference, we denote the positive x-direction as 'downstream', then even the fluid particles just barely outside the slipstream (i.e. $x > 0$ and y slightly greater than $f(x)$) move *upstream*, slowly; they gain speed as they approach the vicinity of the lip, 'turn the corner' and pass across the line source, and move quickly downstream. For $U > 0$, however, the streamline $\psi = 1$ divides the field into two parts: one part is the flow that crosses the line source and enters the slipstream, and the other part is the flow that moves downstream *outside* of the slipstream. As $U \to 1$ the streamline $\psi = 1$ is simply $y = 1$ $(-\infty < x < \infty)$. In that case $f(x) = 1$ and $\gamma_s(x) = \gamma(x) = 1$. It is only in that limiting case that the square-root singularity in γ_s and γ disappears (table 2).

(iv) For the special (important) case $U = 0$, we see from (22) and (23) that the non-dimensional f- and γ-distributions, and hence the streamline pattern, are independent of the 'loading' m/H. It is only the dimensional velocities that vary in proportion to γ_∞ and hence (recall (19)) in proportion to $(m/H)^{\frac{1}{2}}$.

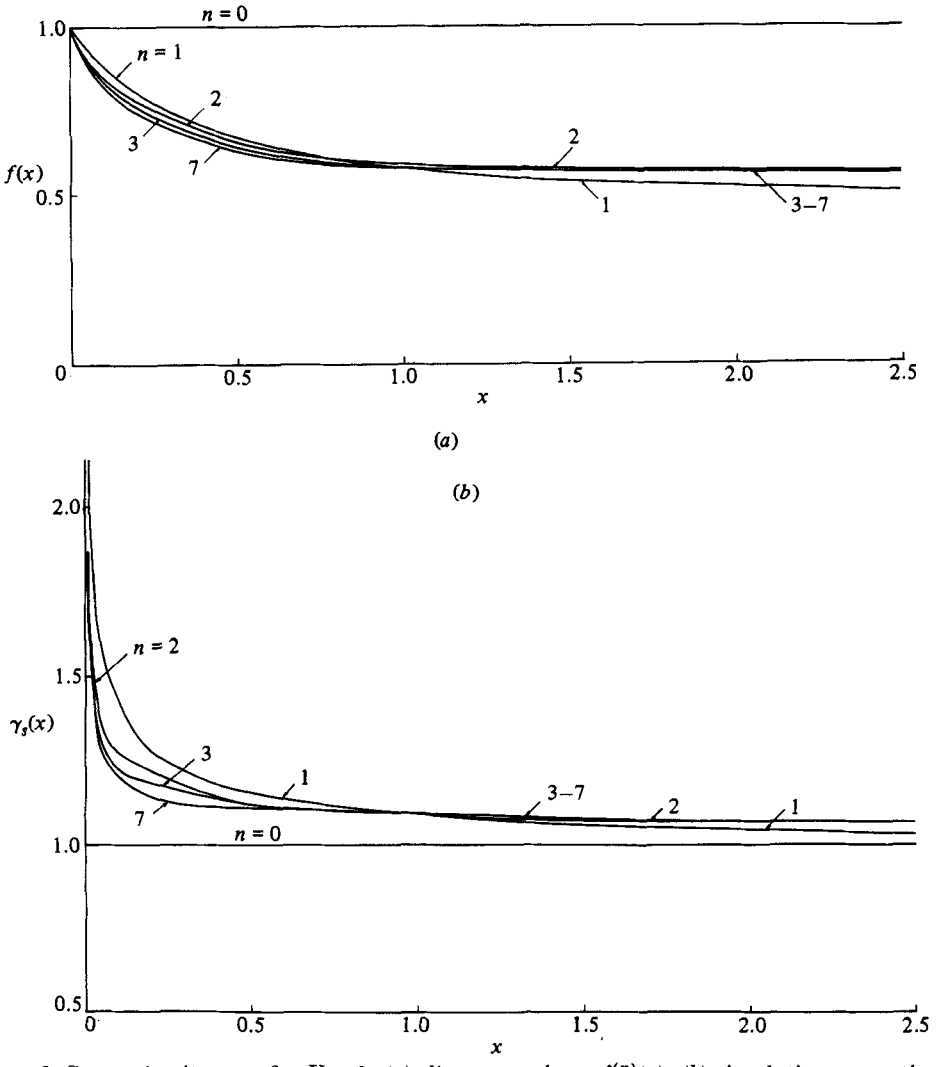

FIGURE 3. Successive iterates for $U = 0$: (*a*) slipstream shape $f^{(n)}(x)$; (*b*) circulation strength per unit arclength $\gamma_s^{(n)}(x)$. Solutions are graphically indistinguishable after the fifth iteration.

(v) Note that $q(0, y) \to \infty$ as $y \to 1$, so that our assumption (6), and the implied result (7), are invalid near the tip of the line source – over $0.97 < y < 1$, say. It is our view that this discrepancy is tolerable since it is so limited in extent.

(vi) The features noted in (i)–(iv) are almost identical with those found in the nonlinear actuator-disk theory (Greenberg 1972), so that one can, at least qualitatively, think of the line-source flow as a plane-flow version of the axisymmetric nonlinear actuator-disk flow.

3. Experiments

3.1. *Experimental design and equipment*

Experiments were designed to study the two-dimensional velocity field of a line momentum source in a 3×4 m shallow water basin 0.3 m deep. The line momentum source is simulated by a large number of closely spaced nozzles mounted on top of

Shape coefficient b_j $j = 1, \ldots, 8$	Circulation coefficient a_j $j = 1, \ldots, 9$	x	$f(x)$	$\gamma_s(x)$
0.218276×10^{-1}	0.177601	0.020	0.9535	1.6815
-0.287096	-0.235269×10	0.040	0.9148	1.3798
0.794853	0.168631×10^2	0.060	0.8824	1.2699
0.478161×10	-0.815639×10^2	0 080	0 8548	1.2174
-0.230399×10^2	0.268108×10^3	0.100	0.8310	1.1895
0.422235×10^2	-0.528318×10^3	0.200	0.7476	1.1476
-0.358453×10^2	0.593562×10^3	0.300	0.6947	1.1298
0.117970×10^2	-0.348323×10^3	0.400	0.6573	1.1160
	0.836881×10^2	0.500	0.6301	1.1079
		0.700	0.5957	1.1020
		0.900	0.5767	1.0959
		1.200	0.5622	1.0830
		1.500	0.5563	1.0753
		2.000	0.5539	1.0693

Collocation points:
x_{kj}: 0.03, 0.08, 0.18, 0.38, 0.68, 1.10, 1.60, 2.20
x_{dj}: 0.02, 0.05, 0.10, 0.18, 0.30, 0.50, 0.80, 1.40, 2.20

TABLE 1. Computed solution of slipstream shape $f(x)$ and circulation distribution $\gamma_s(x)$; $U = 0, f_\infty = 0.5535, \gamma_\infty = 1$

a manifold device placed in a centre channel, with the top flush with the smooth concrete floor of the basin. Specifically, 40 nozzles (made from brass tubes of 3.56 mm inner diameter and 4.2 mm outer diameter), spaced at centre-to-centre distance $s = 25$ mm, discharge high-velocity turbulent jets horizontally at about $h_0 = 4$ mm from the bottom (figure 1). The ratio of the total nozzle cross-sectional area to the cross-sectional area of the manifold is sufficiently small to ensure uniform efflux from all the nozzles. Discharge flow is fed into both ends of the manifold from a constant-head tank, with the same flow withdrawn at the far end of the basin to maintain constant depth during the experiment. Flow rates, large enough to produce measurable velocities near the source, are monitored by two rotameter-type flow meters.

Point velocity measurements are made using a calibrated propeller current meter positioned at mid-depth and mounted on a movable platform which can run along the length of the basin. In addition, streamline and pathline patterns are also recorded photographically against a 20 cm square grid marked on the bottom. The length L of the source, which can be varied by restricting flow from the desired number of nozzles, is made small compared with the basin width W ($L/W < \frac{1}{5}$) in order to essentially eliminate lateral-boundary effects. The experimental parameters for the five experiments carried out with no ambient current are listed in table 3. For further details the reader is referred to Lee (1982).

3.2. *Comparison of theory with experiments*

The flow field, made visible by paper chips on the water surface, is illustrated in figure 6, which shows the observed streamline patterns immediately after the experiment is started, and at steady state. These photographs (exposure 0.5 s) were taken with a Nikon camera mounted 2.3 m directly above the multiple jets. Two start-up vortices are clearly observed at the points of minimum pressure. In the steady flow field the converging sink flow upstream of the source, the separation of the slipstream,

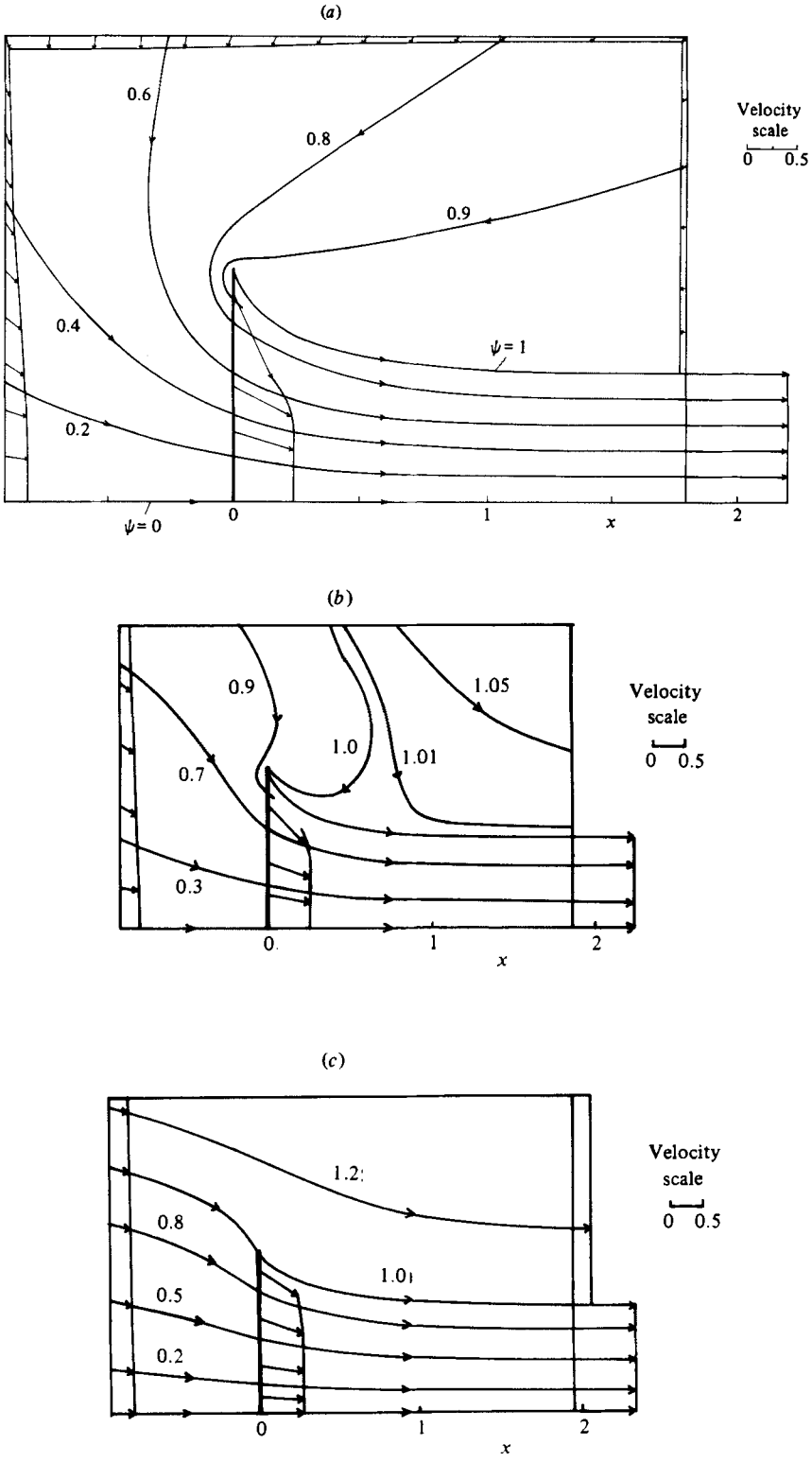

FIGURE 4. Computed streamlines over representative domain: (*a*) $U = 0$; (*b*) 0.1; (*c*) 0.286.

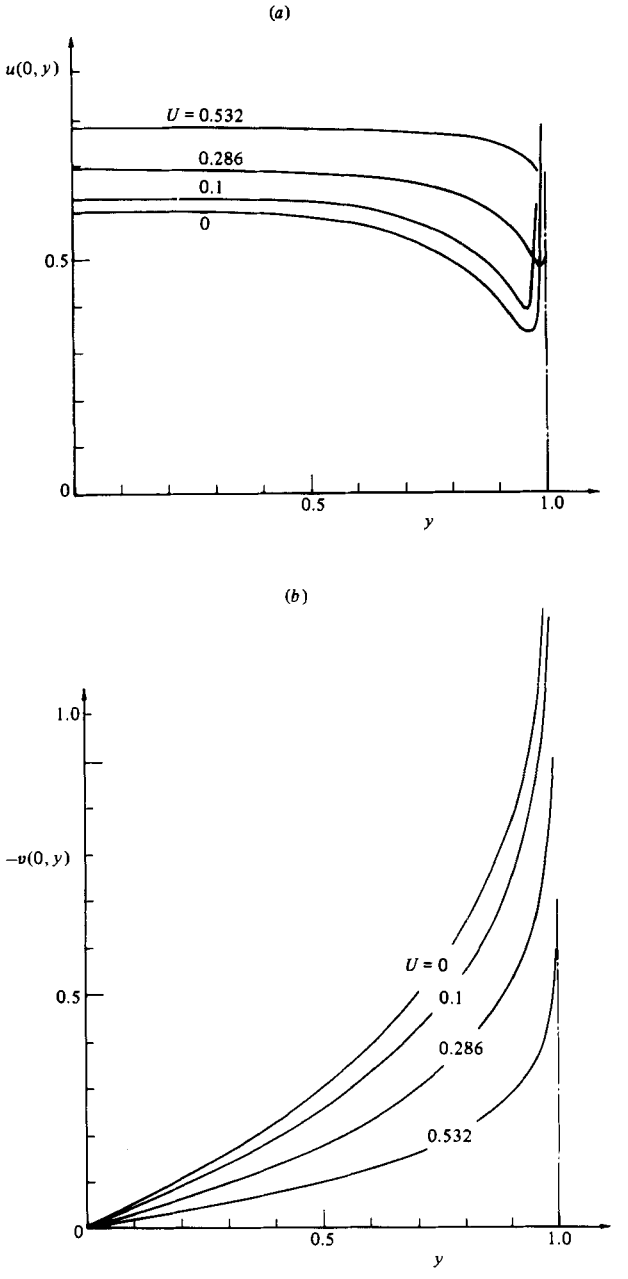

FIGURE 5. Computed velocity distribution at line source: (*a*) $u(0, y)$; (*b*) $v(0, y)$.

and the ultimate jet are all clearly discernible. Observing the shallow-water flow from above (figure 7), two surface depressions (shown schematically as dotted circles) are noted at $y \approx \pm 0.9$, with the end jets strongly bent inwards towards the centre of the jet group. According to our theoretical model, however, the highest velocities, and lowest pressures, occur at the lips $x = 0$, $y = \pm 1$, which is where we would therefore have expected to find the two surface depressions. The experimentally observed displacement of these points to the locations $A(y = -w)$ and $B(y = +w)$ suggests that in our theoretical model the line of pressure discontinuity should be considered to

U	Number of iterations n	a_1	Iteratively computed f_∞	f_∞ given by (34)
0	7	0.177601	0.5535	0.5
0.1	5	0.153505	0.5915	0.55
0.2	5	0.128319	0.6293	0.6
0.286	4	0.984249×10^{-1}	0.6636	0.643
0.532	3	0.323806×10^{-1}	0.7708	0.766
0.7	3	0.154544×10^{-1}	0.8515	0.85
0.8	2	0.960482×10^{-2}	0.9007	0.9

TABLE 2. Variation of number of iterations, circulation singularity strength, and contraction with U

Experiment	Number of nozzles N	Flow rate $Q_0 = Nu_0a_0$ (l/h)	Nozzle spacing s (cm)	Water depth H (cm)	Discharge velocity u_0 (cm/s)	Jet Reynolds number $R_0 = \frac{u_0 D}{\nu}$ $D = 3.56$ mm	$\frac{L}{H}$	u_∞ (cm/s)
1	20	600	2.5	2.0	83.9	2980	26.4	16.7
2	20	750	2.5	2.0	104.9	3730	26.4	20.9
3	20	900	2.5	2.0	125.9	4480	26.4	25.1
4	24	750	2.5	2.4	87.4	3110	24.0	15.6
5	24	1050	2.5	2.4	122.4	4350	24.0	22.3

TABLE 3. Summary of experimental parameters

extend from A to B (figure 7). (Recall that we have neglected the three-dimensionality of the flow in the momentum-transfer region and, *a priori*, adopted the source length L as the length of the line of pressure discontinuity in our formulation.) The entire theoretical development leading to the dimensionless governing equations (31) and (32), along with the results given in §2, remains intact – except that the non-dimensionalizing length $\frac{1}{2}L$ is replaced by w. Further, we note that the dimensionless width of the ultimate jet $f_\infty/0.5L$ is given exactly by the global momentum balance (34) regardless of the flow details near the source. Consequently, this physical interpretation of our model permits a prediction of the location of the slipstream lips as

$$\frac{w}{0.5L} = \frac{0.5}{f_\infty}(1+U), \tag{35}$$

where f_∞ is iteratively computed from (31) and (32) (table 2). Equation (35) and the numerically computed f_∞ (table 2) show that for the strongest slipstream contraction, namely the case $U = 0$, we have $w/0.5L = 0.9$, and that the slipstream lips approach the ends of the source as U increases.

The measured and computed flow fields agree in all of their main features, and quantitatively the agreement is to within differences of around 10 %. The fact that such converging flow geometries, qualitatively quite similar to the classical Borda mouthpiece, can arise in the vicinity of high-velocity jets discharged in proximity to the free surface has also been pointed out previously by Streiff (1950) in connection with test results of model underwater spilling tubes.

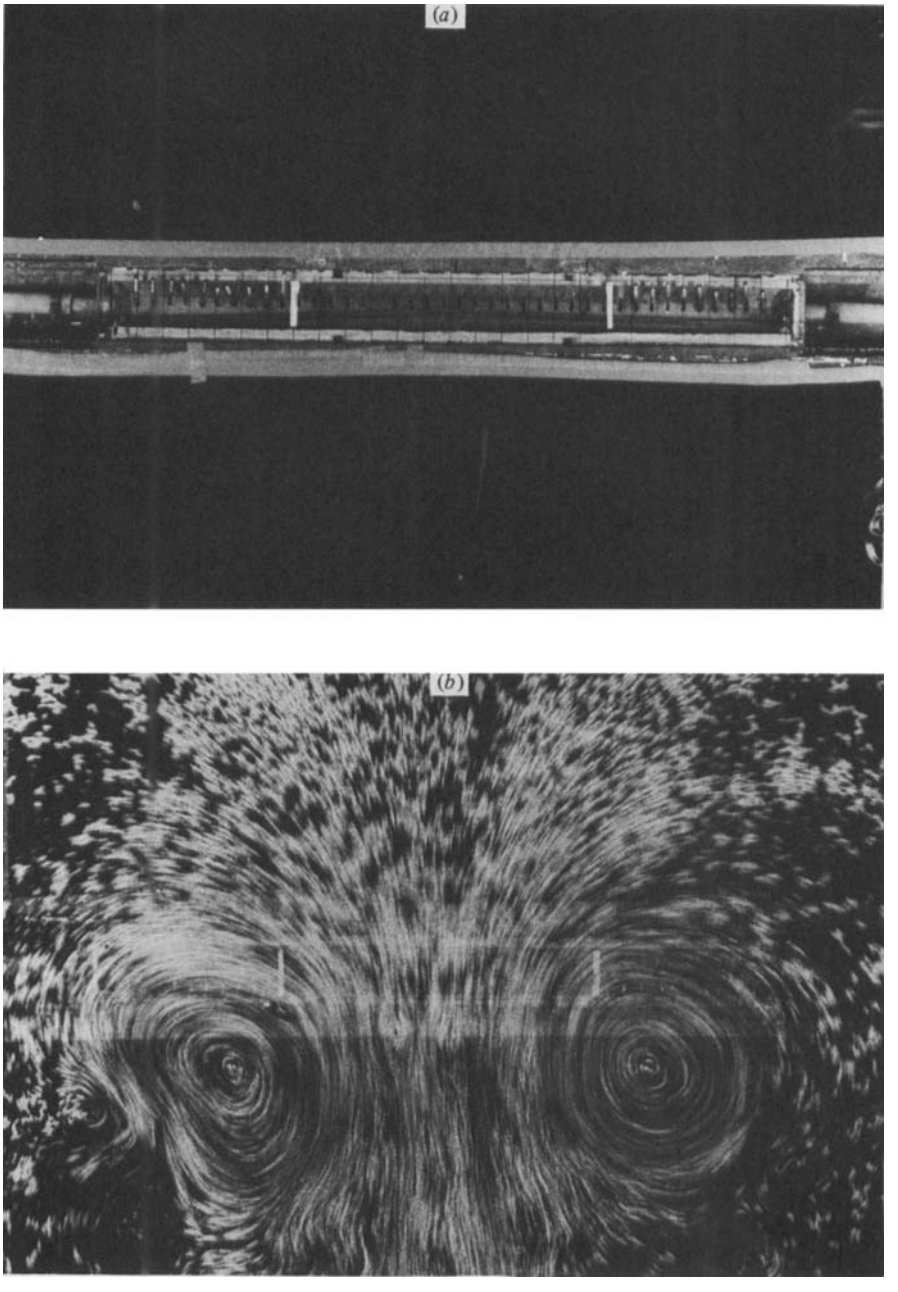

FIGURE 6(*a*, *b*). For caption see facing page.

The velocity profile across the ultimate jet (figure 8) at $x = 2$ shows a plateau region about half the width of the line source, with a sharply falling edge indicative of turbulent diffusion – a real-fluid effect not accounted for in our present formulation. Maximum velocities are, in general, around 10% below predicted values. The computed x-velocity at the source, $u(0, y)$, is compared with the experimental measurements in figure 9(*a*). Here the non-dimensionalizing u_∞ is taken to be the average measured velocity in the plateau region of the ultimate jet, and $u(0, y)$ is the

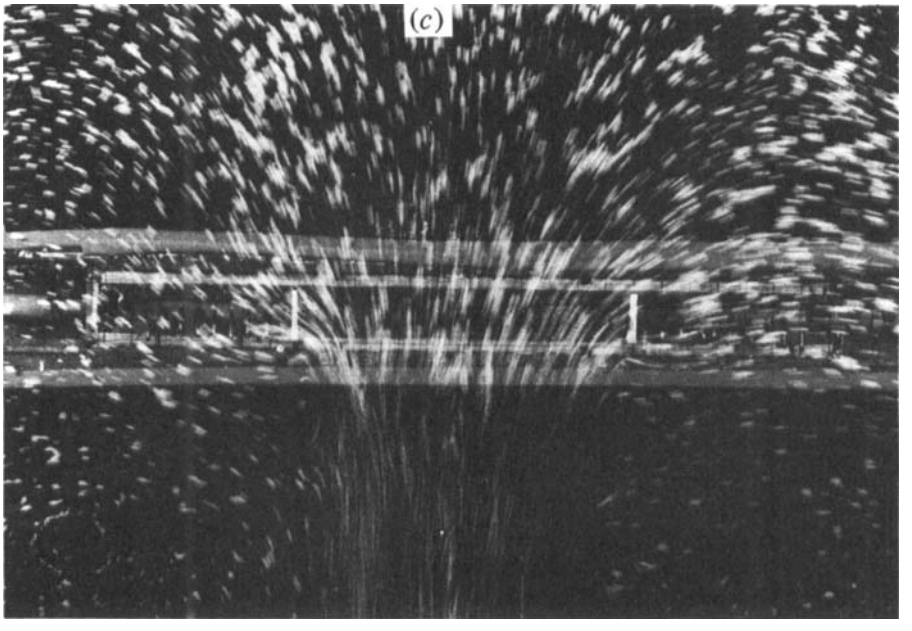

FIGURE 6. (*a*) Top view of multiple-nozzle arrangement for simulation of line momentum source (experiment 3); end nozzles are indicated by bright stripes. (*b*) Observed start-up vortices near $x = \pm 0.5$ immediately after start of experiment (experiment 3). (*c*) Steady streamline patterns of a line-momentum-source-induced flow (experiment 3).

average of the measured velocities at two symmetrical y-positions. The y-velocity cannot be measured at $x = 0$ owing to the obstruction of the nozzles. Measurements of v at $x = -0.16$ show the same sort of agreement when compared with predicted velocities in figure 9(*b*).

Because of the relatively small size of the present laboratory basin, experiments with a uniform coflowing current cannot be satisfactorily performed. However, previous experimental observations of flow patterns by Lee, Jirka & Harleman (1977) for a wider range of L/H in a much larger hydraulic model basin do indicate at least qualitative agreement with the calculated flows. In particular, for $U = 0.046$ a clear inward-directed sink flow from the surrounding fluid upstream of the multiple jets is noted, in accord with the present computations.

The results of this study suggest that a further comprehensive experimental investigation of line momentum sources in an ambient current is warranted. Detailed velocity measurements at key points in the induced flow in a large experimental basin will be a worthwhile undertaking.

4. Concluding remarks

Multiple jets in confined depth have been treated as a line momentum source in this study. In the presence of a free surface the induced flow is predominantly two-dimensional, and can be calculated by a line-vortex model of the slipstreamlines. The computed flow, which is quite different from that of classical free jets, is shown to be accurate up to very close to the slipstream lips.

Whereas the effect of jet buoyancy has not been addressed in this paper, the present results are applicable for multiple weakly buoyant jets into restricted depths, such

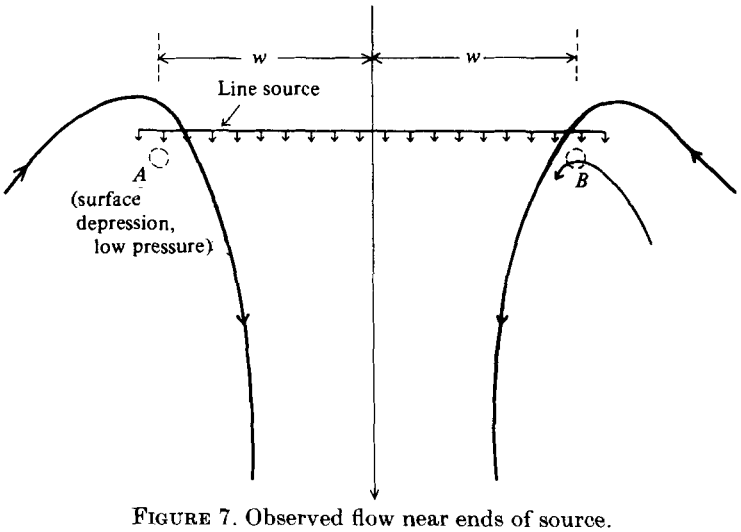

FIGURE 7. Observed flow near ends of source.

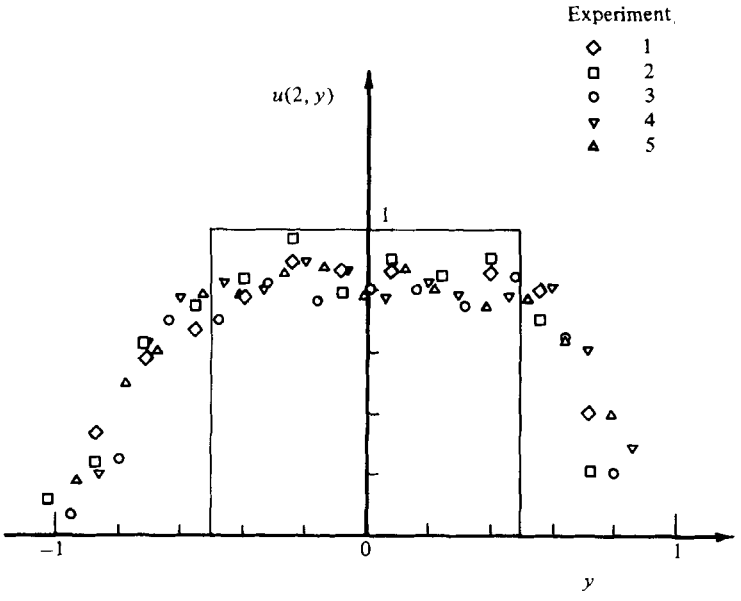

FIGURE 8. Measured velocity profile at $x = 2$ (all lengths non-dimensionalized by the half-source length $0.5L$).

as cooling-water discharges into shallow receiving waters. Jirka & Harleman (1979) and Lee & Jirka (1980) have shown that weakly buoyant jets in confined depth tend to exhibit an unstable configuration, and become uniformly mixed over the ambient depth. As a first approximation it is often possible to neglect the discharge buoyancy altogether, so that the flow dynamics near the source are governed purely by the momentum source represented by the high-velocity injection.

The success of the present theoretical approach suggests extension to the case in which the ambient current is misaligned with the source momentum.

Only towards the completion of this paper did we come across a somewhat related

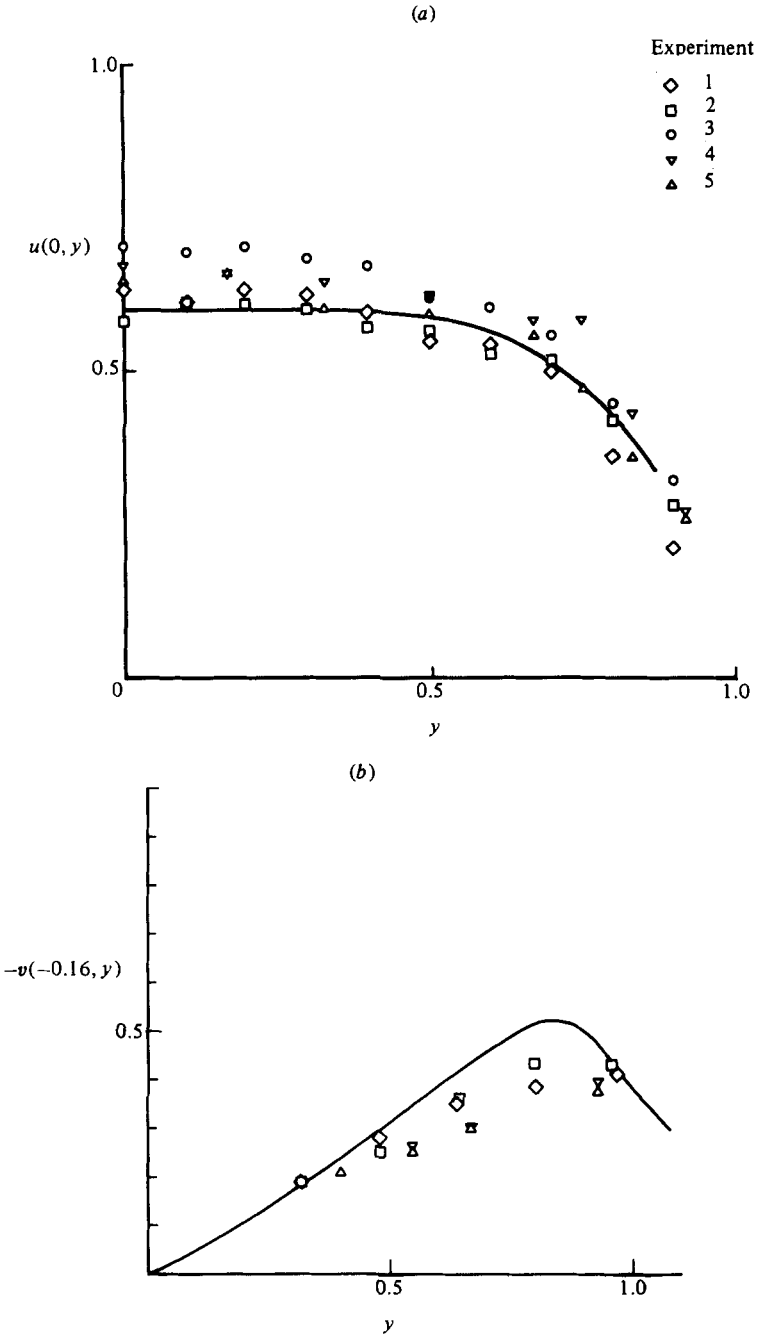

FIGURE 9. Comparison of predicted velocities near momentum source with experimental values: (*a*) x-velocity at source line; (*b*) y-velocity at $x = -0.16$.

work by Lighthill (1979) in connection with animal hovering in ground effect. In his paper a plane version of the classical actuator-disk model is modified by the inclusion of an artificial vertical boundary to shield the slipstream from the outside sink flow. The fluid motion induced by the hovering object in still air is then obtained by conformal mapping, and its resemblance to the Borda-mouthpiece flow patterns are

discussed. The theoretical approach in the present paper circumvents the need for such an artificial boundary.

This work was supported by an Engineering Research Initiation Grant from the U.S. Engineering Foundation and in part by a research grant from the University of Hong Kong. All numerical computations were done on an IBM 3031 machine at the Computer Center of the University of Hong Kong. The writers are indebted to their colleague Mr Y. K. Poon for carrying out the experiments.

REFERENCES

ABRAMOVICH, G. W. 1963 *The Theory of Turbulent Jets*. MIT Press.

ALBERTSON, M. L., DAI, Y. B., JENSEN, R. A. & ROUSE, H. 1950 Diffusion of submerged jets. *Trans. ASCE* **115**, 639–664.

BAINES, W. D. & KEFFER, J. F. 1974 Entrainment by a multiple source turbulent jet. *Adv. Geophys.* **18B**, 289–298.

DAVIS, M. R. & WINARTO, H. 1980 Jet diffusion from a circular nozzle above a solid plane. *J. Fluid Mech.* **101**, 201–221.

FISCHER, H. B., LIST, E. J., KOH, R. C. Y., IMBERGER, J. & BROOKS, N. H. 1979 *Mixing in Inland and Coastal Waters*. Academic.

GREENBERG, M. D. 1972 Nonlinear actuator disk theory. *Z. Flugwiss.* **20**, 90–98.

JIRKA, G. H. & HARLEMAN, D. R. F. 1979 Stability and mixing of a vertical plane buoyant jet in confined depth. *J. Fluid Mech.* **94**, 275–304.

KNYSTAUTAS, R. 1964 The turbulent jet from a series of holes in line. *Aero. Q.* **15**, No. 1.

LAMB, H. 1932 *Hydrodynamics*, 6th edn. Dover.

LEE, J. H. W. 1980 Near field flow generated by a thermal diffuser in shallow water. In *Proc. 10th Southeastern Conf. on Theor. and Appl. Mech., Tennessee, April 1980*, pp. 373–396.

LEE, J. H. W. 1982 Multiport thermal diffusers as line momentum sources in shallow water. *US Engng Found. Rep. Grant* RC-A-78-6A.

LEE, J. H. W. & JIRKA, G. H. 1980 Multiport diffuser as line source of momentum in shallow water. *Water Resources Res.* **16**, 695–708.

LEE, J. H. W. & JIRKA, G. H. 1981 Vertical round buoyant jet in shallow water. *J. Hydraul. Div. ASCE* **107** (HY12), 1651–1675.

LEE, J. H. W., JIRKA, G. H. & HARLEMAN, D. R. F. 1977 Modelling of unidirectional thermal diffusers in shallow water. *MIT Parsons Lab. Rep.* 228.

LIGHTHILL, J. 1979 A simple fluid-flow model of ground effect on hovering. *J. Fluid Mech.* **93**, 781–797.

MILLER, D. R. & COMINGS, E. W. 1960 Force-momentum fields in a dual jet flow. *J. Fluid Mech.* **7**, 237–256.

SCHLICHTING, H. 1968 *Boundary Layer Theory*. McGraw-Hill.

STREIFF, A. 1950 Discussion of 'Diffusion of submerged jets'. *Trans. ASCE* **115**, 684–687.

TAYLOR, G. I. 1958 Flow induced by jets. *J. Aero. Sci.* **25**, 464–465.